Proceedings of the Korean Nuclear Society Autumn Meeting
Seoul, Korea, October 2001

Development of Predicting Model for Sodium Coolant Boiling

Won-Pyo Chang, Dohee Hahn

Korea Atomic Energy Research Institute
P.O.Box 105, Yusung, Taejon, Korea

Abstract

Sodium coolant boiling is a safety concern in Liquid Metal Reactors using sodium as coolant. It affects the safety through the void reactivity feedback and heating up the fuel rod. The present model is being developed to meet the demand for predicting the void fraction as well as the fuel and cladding temperatures in the KALIMER, to analyze the damage of the fuel rods core after onset of sodium boiling. Modeling of the sodium boiling was basically issued because the model adopted in Light Water Reactor systems were not proper to be directly applied to the sodium coolant reactors, mainly due to the phenomenon difference observed between two types of coolant systems. The developing model is a multiple-bubble slug ejection model. It allows a finite number of bubbles in a channel at any time. Voiding is assumed to result from formation of bubbles that fill the whole cross section of the coolant channel except for liquid film left on the cladding surface. The vapor pressure, currently, is assumed to be uniform within a bubble. The present study is focused on not only demonstration of the sodium voiding behavior predicted by the developed model, but also confirmation on the qualitative acceptance. In a result, the model catches the key phenomena for sodium boiling, continuous effort, however, should be made for the complete analysis.

1. Introduction

The Korea Atomic Energy Research Institute (KAERI) has been developing the conceptual design of KALIMER (**K**orea **A**dvanced **LI**quid **ME**tal **R**eactor) [1], which is a sodium cooled, 150 MWe, pool-type reactor. The primary heat transport system (PHTS) of KALIMER is submerged in the big sodium pool, which provides the large thermal inertia of the system. KALIMER, with a metallic fueled core, is designed in such a way that intrinsic negative reactivity feedback effect is expected

during the transients including design basis events.

Even though the KALIMER design may not allow boiling at any circumstance under the design basis accidents, sodium boiling is anticipated under HCDA (Hypothetical Core Disruptive Accident) initiating events which are represented by UTOP (Unprotected Transient Over Power), ULOF (Unprotected Loss Of Flow), ULOHS (Unprotected Loss Of Heat Sink), or sudden flow channel blockage, due to power excursion caused by the reactivity feedback. For realistic assessment of the HCDA consequence, it is also important to predict the core void in order to estimate the core reactivity feedback.[2] The slug and annular flow regimes tend to prevail for liquid-metal boiling near atmospheric pressure, while the bubbly flow is typical under high pressure in light water reactors.[3,4] In this regard, sodium voiding in liquid metal reactors should be modeled because of phenomenon difference between two reactor systems. Unfortunately, SSC-K [5] which is used as the main code for KALIMER safety analysis is not capable of analyzing the sodium boiling so far. To this end, the sodium boiling model has been developed in order to extend the applicable range of SSC-K.

There are a few codes capable of analyzing the HCDA initiating events. SAS series [6] and FRAX [7,8,9] codes may be representatives on this area. They basically use the multi-bubble slug ejection model, which represents the boiling coolant with multi liquid slugs divided by bubbles.

2. Theory for Sodium Boiling Model (SOBOIL)

Sodium boiling model in SOBOIL is basically multi-bubble slug ejection model similar to that used in SAS2A.[4] Since the interfaces between the liquid slugs and a vapor bubble are moving, a model which uses only fixed nodes is not be likely to be good enough. Voiding is assumed to result from formation of bubbles that fill the whole cross section of the coolant channel except for liquid film left on the cladding or structure. A finite number of vapor bubbles, separated by liquid slugs, are allowed in the channel at any time. The liquid film around the vapor is assumed to be static currently, its motion, however, will be improved later.

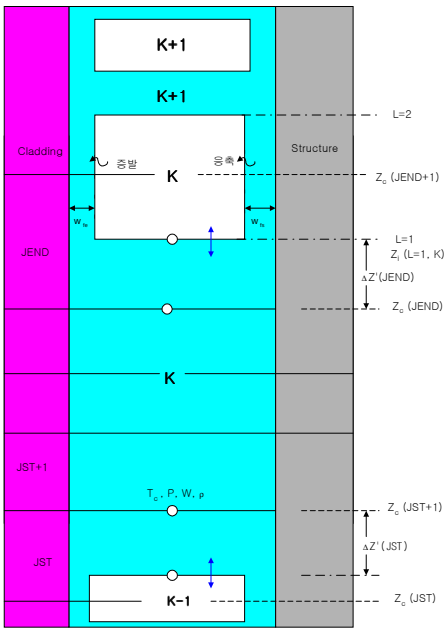

Fig. 1 Nodalizations for 'SOBOIL' Model

(1) Liquid Slug Flow Rates

The description of the momentum conservation equation for the liquid flow is similar to that used in SAS2A, except expressing it with flow rate instead of mass flux in order to take account of the flow area variation for a node in the numerical computation. The integral liquid momentum equation is given by

$$\frac{1}{A_c}\frac{\partial W}{\partial t} + \frac{\partial P}{\partial z} + \frac{1}{A_c}\frac{\partial (Wv)}{\partial z} = -\left(\frac{\partial P}{\partial z}\right)_{fr} - \left(\frac{\partial P}{\partial z}\right)_{K} - p_c g \tag{1}$$

The momentum equation is applied to each slug which is represented in the Fig. 1, individually, and is integrated over the length of each slug rather than over the length of the channel. One can obtain

$$I_1 \frac{\partial W}{\partial t} + P_t - P_b + W^2 \; I_2 + A_{fr} \; W|W|^{\,1+b_{fr}} \; I_3 + W|W| \; I_4 + g \; I_5 = 0 \tag{2}$$

where,

$$\mathrm{I}_1 = \int \frac{dz}{\mathrm{A}_C} = \sum_{JC=JST}^{JEND} \mathrm{X}_{I1}(JC), \qquad \mathrm{X}_{I1}(JC) = \frac{\Delta z \;(JC)}{\mathrm{A}_C(JC)} \tag{3}$$

$$\mathrm{I}_2 = \sum_{JC=JST}^{JEND} \mathrm{X}_{I2}(JC), \qquad \mathrm{X}_{I2}(JC) = \frac{1}{\mathrm{A}_C(JC)^2}\left[\frac{1}{\rho_C(JC+1)} - \frac{1}{\rho_C(JC)}\right] \tag{4}$$

$$\mathrm{I}_3 = \int \frac{1}{2\rho_C \mathrm{A}_C^2 D_h}\left[\frac{D_h}{\mu \mathrm{A}_C}\right] b_{fr} \; dz = \sum_{JC=JST}^{JEND} \mathrm{X}_{I3}(JC) \tag{5}$$

$$\mathrm{X}_{I3}(JC) = \frac{\Delta z \;(JC)}{\left[\rho_C(JC) + \rho_C(JC+1)\right]\mathrm{A}_C(JC)^2 D_h(JC)}\left[\frac{D_h(JC)}{\overline{\mu}(JC)\mathrm{A}_C(JC)}\right]^{b_{fr}}$$

$$\mathrm{I}_4 = \sum_{JC=JST}^{JEND} \mathrm{K}_{OR}(JC) \tag{6}$$

$$\mathrm{I}_5 = \int \rho_C \; dz = \sum_{JC=JST}^{JEND} \mathrm{X}_{I5}(JC), \quad \mathrm{X}_{I5}(JC) = 0.5\left[\rho_C(JC) + \rho_C(JC+1)\right]\Delta z(JC) \tag{7}$$

The integer variable JST is the number of the mesh segment in which the bottom of the liquid slug is located, while JEND is the number of the segment in which the top is contained. All I's in Eq. (2) except I_5 are assumed to be constant over the time step because the liquid interface density is considered to be a very small effect and can be neglected. Since the interface location changes with time,

$$\mathrm{I}_5(t) = \int_{z_{JST}(t)}^{z_{JEND}(t)} \rho_\lambda(z)\, dz \tag{8}$$

and at t + Δt,

$$\mathrm{I}_5(t+\Delta t) = \int_{z_{JST}(t+\Delta t)}^{z_{JEND}(t+\Delta t)} \rho_\lambda(z)\, dz \tag{9}$$

Taking the difference for these two variables

$$I_5(t+\Delta t) - I_5(t) = \int_{z_{JEND}(t)}^{z_{JEND}(t+\Delta t)} \rho_\lambda(z)\, dt \; - \int_{z_{JST}(t)}^{z_{JST}(t+\Delta t)} \rho_\lambda(z) dz \qquad (10)$$

because these two integrals, Eq. (8) and Eq. (9) are identical except in segment JST and JEND, where the bubble interface positions are changing with time.

(2) Liquid Temperature

Since the interface moves along the axis, both Eulerian and Lagrangian schemes are used for computing transient temperatures in the liquid coolant. The Eulerian scheme is usually applied before incipient boiling, while the Lagrangian scheme is used for all liquid slugs other than the inlet liquid slug after boiling. However, Lagrangian scheme is also used for the inlet liquid slug with a low flow rate (~ 10 % of the initial flow rate).

For the Eulerian scheme, the basic energy equation in a liquid slug is given by

$$\rho_l c_l \frac{\partial T_c}{\partial t} + G c_l \frac{\partial T_c}{\partial z} = \varphi(z,t) + Q_c(z,t) \qquad (11)$$

Eq. (11) is numerically discritized with semi-implicit method in time and space.

For the Lagrangian scheme, it is used to calculate the liquid coolant temperatures both at the fixed axial mesh points and at the moving points near the liquid-vapor interfaces. The Lagrangian total time derivative, dT_c / dt, as seen by an observer moving with the coolant velocity, is used and axial heat conduction through the interfaces is ignored in the calculation. This derivative is approximated by

$$\frac{dT_c}{dt} = \frac{T_c(z, t+\Delta t) - T_c(z-\Delta z, t)}{\Delta t} \qquad (12)$$

where

$$\Delta z = \frac{[G(t+\Delta t) + G(t)]\Delta t}{2\bar{\rho}(z)}, \qquad \bar{\rho}(z) = \rho(\, T_c(z, t+\Delta t/2)\,) \qquad (13)$$

(3) Bubble Formation and Collapse

a. Basic Assumptions for Vapor Bubble Modeling

The present SOBOIL model has been developed based on the uniform pressure model which is adequate to small bubbles. For small bubbles, the pressures may be assumed to be uniform spatially

inside the bubbles, whereas there exists a pressure gradient for a bubble length exceeding the specified minimum size. Thus, a different model must be applied because axial distribution of the pressure cannot be ignored. This model, however, will be considered in the present model.

Vapor is formed if a specified amount of superheat is satisfied at a node in the model. If the specified amount of superheat is exceeded in a node, then time-step size is reduced, and coolant calculations for the channel are repeated for the time step, so as to satisfy the superheat criterion exactly at the end of time step. This model, however, is subjected to the following limitations.

(i) If new vapors are formed in a channel, the maximum of 9 bubbles are allowed ;

(ii) No new vapors will be formed within a minimum distance adjacent to a vapor-liquid interface, and, thus, nodes within the distance from the interface are not examined for bubble formation ;

(iii) No more than one bubble will be formed within a time-step

(iv) Vapors are always saturated at given temperatures.

(v) If a vapor temperature change exceeds a specified amount, the time-step is also reduced.

(vi) A new vapor generated in a liquid slug divides the liquid slug into two liquid slugs and the initial liquid flow rates for these two liquid slugs are assumed same as that of the liquid slug before the voiding.

Fig. 3 shows the control volume considered in the uniform vapor pressure model. Vapors are assumed to fill the whole cross section of the coolant channel, except for a liquid film left on the cladding or structure. The shrink of a vapor bubble is possible because of condensation in the cooler region. When vapor length and decreasing rate of the size are simultaneously below the minimum values, the vapor disappears. Two liquid slugs are also combined into one if the gap between two vapors is close enough each other.

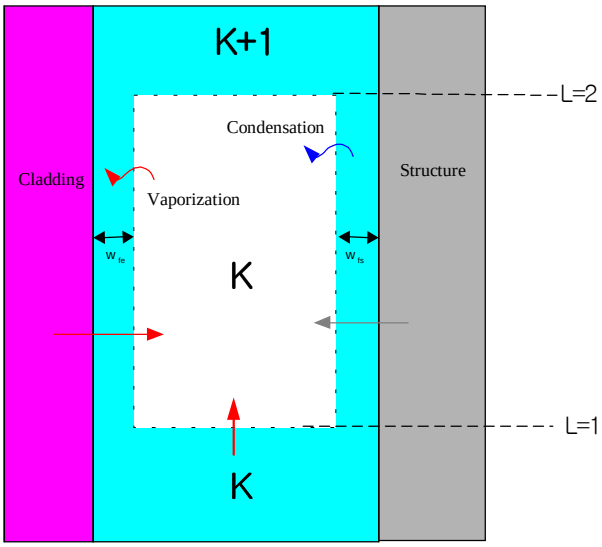

Fig. 3 Uniform Pressure Vapor Model

The bubble growth is determined by coupling the momentum equations for the liquid slugs with an energy balance in the vapor bubble, assuming saturation conditions and spatially uniform pressure and temperature within a vapor. The rate of formation and condensation of a vapor is determined by the heat flow through the liquid film on the cladding or structure, and through the liquid-vapor interfaces. The primary focus of this model is to obtain the temperatures within vapor bubbles. Once temperatures are known, it can be used to calculate the vapor pressures, since saturation conditions are

assumed. The vapor pressure is the driving force for the motion of the liquid slugs, so finding the vapor pressures in all bubbles provides the link between conditions in the liquid slugs and conditions in the vapors. Therefore the vapor pressure leads to a complete description of conditions throughout the channel.

(4) Energy transfer into uniform pressure bubble

The total energy added to vapor bubble K in a time step is

$$Q_t = \int_t^{t+\Delta t} [\, Q_{es}(\tau) + Q_i(\tau) \,]\, d\tau \tag{14}$$

Q_{es} is the heat flow from the heat structure and approximated by

$$Q_{es} = \frac{\Delta t}{2}\left[Q_{es}(k,t) + Q_{es}(k,t+\Delta t) \right] \tag{15}$$

where,

$$Q_{es}(k,t) = P_e \int_{Z_i(L=1,t,K)}^{Z_i(L=2,t,K)} q_e(z,t)\, dz \tag{16}$$

(5) Heat Flow through Liquid-vapor Interface

Calculation of interfacial heat transfer between liquid and vapor in SOBOIL model is directly based on that in SAS2A [2]. In this method, total heat flow through the liquid-vapor interfaces is the sum of an upper interface term I_{iu} and a lower interface term I_{il}

$$Q_i = \Delta t\left(I_{iu} + I_{il} \right) \tag{17}$$

where

$$I_{ix} = k_l A_{cx} \left. \frac{\overline{\partial T}_{lx}}{\partial \xi} \right|_{\xi=0} \tag{18}$$

with

x = u or l

A_{cx} = Area of coolant channel

T_{lx} = Liquid temperature near interface

ξ = Axial distance from interface

ξ = $z - z_i$ for upper interface

ξ = $-(z - z_i)$ for lower interface

$\overline{\frac{\partial T_l}{\partial \xi}}_x$ = Time average of the spatial derivative for the time step. An expression for the coolant temperature derivative $\overline{\frac{\partial T_l}{\partial \xi}}_x$ can be derived from the general heat conduction equation;

$$\alpha \frac{\partial^{2T_2}(\xi,\ t')}{\partial \xi^2} + \frac{Q(\xi,\ t')}{\rho_2 C_2} = \frac{\partial T_l(\xi,\ t')}{\partial t'} \tag{19}$$

The boundary conditions for the problem are:

$T_l(\xi = 0,\ t') = T(t')$, the liquid temperature at the liquid-vapor interface

$T_l(\xi = \infty,\ t') \quad < \infty,$

The initial condition is:

$T_l(\xi, t' = 0)$ *known*

The heat conduction equation, Eq. (19), together with the initial and boundary conditions, can be solved for T_l using the Laplace transform method.

(6) Change in Vapor Energy

The heat flow into the vapor control volume is used both to produce new vapor and to raise the temperature of already existing vapor. During a time interval Δt, the vapor temperature goes from T to $T+\Delta T$, the pressure goes from $P_V+\Delta P$, the density goes from $\rho_V + \Delta\rho_V$, the bubble volume goes from V_v to $V_v + \Delta V$, and the vapor energy changes by ΔE. The $\triangle P$ and $\triangle \rho_v$ are related to $\triangle T$ by the requirement that saturation conditions prevail in the vapor.

Two processes contribute to energy change $\triangle E$. One is the heating of the quantity of vapor present at the beginning of the time step from temperature T to temperature $T+\triangle T$. The other is the vaporization of some of the liquid film to an additional vapor, giving a total vapor mass of $(\rho_v + \triangle\rho_v)$ $(V_v+\triangle V)$ at the end of the time step. However, it is not straightforward to formulate an expression for the energy change by directly considering the heating of the vapor (because of the volume and density changes which take place during the heating) and the vaporization of some liquid film (because the

amount of film vaporized is unknown). Therefore, a thermodynamically equivalent path is considered instead of straightforward expression of the energy change. This path can be described in the following three steps:

Step 1: condense the vapor in the bubble at time t to liquid at constant pressure and temperature

Step 2 : heat the liquid from step 1 to T+△T:

Step 3 : vaporize the liquid from step 2 plus enough liquid from the film to fill the volume V_v+△V:

(7) Energy Balance

The energy balance between the energy transferred to the control volume and the energy change within the volume, determines change of the vapor energy. The energy transferred to the volume, E_t, is sum of energy flow from the cladding or structure, Q_{es}, and the energy flow through the liquid-vapor interfaces, Q_i, in Eq. (17). E_t can further be expressed as a linear function of the change in the vapor temperature, ΔT.[10] When E_t is combined with ΔE together, the resulting equation is a linear equation in terms of the changes in the vapor temperatures of bubbles K-1, K, and K+1, which may be arranged as:

$$C_1(K)\Delta T(K-1) + C_2(K)\Delta T(K) + C_3(K)\Delta T(K+1) = C_4(K) \quad (31)$$

In general, if a series of N bubbles of uniform vapor pressure extends from the bottom to top of the channel, then temperature changes in the N bubbles are calculated by solving a set of linear equations written in terms of N unknowns. Once the vapor temperatures are known, the saturation conditions are used to obtain the vapor pressures.

4. Results

The KALIMER design parameters for the core channel are used for the model development. The initial values for SOBOIL are obtained from the steady state results of the ULOHS analysis using SSC-K. The main parameters used in the verification of the developed SOBOIL model are summarized in Table 1. Fig. 5 represents the schematics of the KALIMER fuel pin modeled by SOBOIL.

Table 1 Parameters for SOBOIL verification

Parameters	Values used in SOBOIL	Parameters	Values used in SOBOIL
Core Height (m)	3.930	Fuel Pallet Radius (m)	2.73×10^{-3}
Flow Area (m^2)	2.87×10^{-5}	Cladding Inner Radius (m)	3.15×10^{-3}
Hydraulic Diameter (m)	2.87×10^{-5}	Cladding Outer Radius (m)	3.70×10^{5}
Perimeter (m)	0.0074	Time-Step (ms)	5.0
Initial Liquid Flow (kg/s)	0.14686	No. of Axial Nodes	67
Inlet Coolant Temp. (^oK)	1150.70	No. of Radial Nodes	6
Inlet Coolant Pressure (Pa)	4.30×10^{5}	in the Fuel Pallet	
Outlet Coolant Pressure (Pa)	1.610×10^{-5}	No. of Radial Nodes	6
		in the cladding	

The fuel pin consists of 4 regions, i.e. lower plug, fuel slug, upper gas plenum, and upper plug. Fig. 6 is the steady state temperatures for the cladding surface and liquid coolant in the channel. The coolant and cladding surface temperatures exhibit the expected profiles. The temperature suddenly drops at the node # 41, which corresponds to the end of the fuel slug region, because there is no heat generation in the upper gas plenum region. Heat is generally generated in the fuel slug region but heat transfer should be considered in the upper gas plenum region, because the gas temperature inside the upper plenum gas region changes depending on the cladding temperature. In SOBOIL, however, the gas temperature is assumed to be same as that of the inner cladding surface temperature, which means that an adiabatic boundary condition is applied. The gas heat capacity is considerably small compared with that of the cladding material so that this assumption would not deviate far from the reality while great effort on the numerical problems is avoided.

For the transient, the core inlet coolant temperature is assumed to increase 50 ^oK/sec while the inlet coolant pressure keeps the same value as given in Table 1, taking account of a condition during the ULOHS accident. As a newly generating vapor gets the saturation pressure corresponding to the specified superheated temperature of the liquid coolant corresponding to the vapor generation criteria, the vapor pressure is higher than the liquid pressure at that point by amount of the superheat. Consequently, pressure jump is anticipated when a new vapor is generated in the present model. Fig. 7 is the result of the pressure change for the first vapor with time. The vapor pressure indeed made a jump from the initial liquid pressure, 0,168 MPa to over than 0.176 MPa. Then, the vapor pressure initially goes down. It may be probably due to the heat transfer from the vapor to the cladding surface in the vapor region. Since the heat capacity of the cladding is larger than sodium, the cladding temperature does not change much while the coolant temperature gets higher because of the coolant inlet boundary condition. Therefore, heat usually transfers from the vapor to the cladding surface. The liquid temperature near the interface between the vapor and liquid coolant is also to be higher than the

cladding temperature, and, consequently, it reduces the liquid coolant temperature so that heat flow occurs from vapor to the liquid slug at the interface. These two heat flows make the vapor pressure down together with the vapor volume expansion in the early period. The slightly negative wall heat flow and positive interface heat transfer are observed in the early time in Fig. 8 and Fig. 9. It explains these heat transfers are directed out of the vapor. The positive interfacial heat transfer indicates energy is transferred from the vapor to the liquid because of the coordinate system used in Eq. (19). The vapor pressures strongly depends on the heat transfers as seen Fig. 8, 9. The vapor pressure is likely to be very sensitive to the heat transfer from the vapor to the wall and interfaces. As the vapor gets larger and amount of the heat transfer from the vapor to the wall (cladding surface) also begins larger than the heat transfer from the vapor to the liquid slug at the interface. In result, the vapor pressure is quickly reduced as seen in Fig. 7. The sudden changes of the vapor pressure and heat transfers after about 2.25 second, however, are not clearly understood at this time. Further study is necessary.

Fig. 10 presents the growth of the first generated vapor size. The vapor size increases within a short time. As the first bubble forms at the end of the channel, the upper interface of the vapor locates at the exit. Thus only the lower interface gets to grow downward. The fast increase of the vapor pressure is also likely to cause the lower interface of the vapor to move downward rapidly. The strange behavior of the interface around 2.3 second is not fully understood either, but it looks like being implicitly linked with the liquid slug flow below the vapor as well as the vapor pressure change. It is also noted that when the vapor size exceeds a certain value, the wall heat flow plays a major role in the pressure change of the first vapor. It's behavior in Fig. 7 after 2.25 may come from such sensitive response of the vapor pressure to the wall heat transfer. It presumably gives rise to the stability problem and further calculation fails. The result of the liquid flow is shown in Fig. 11. The sudden jump for the liquid flow after 2.3 second is considered to come from two reasons. The first one is the pressure change of the first vapor and the other one is rapid expansion of the second vapor generated below the first one.

Fig. 12 represents the second vapor growth. The upper interface develops more quickly then the lower one and it approaches to the first bubble and, subsequently, the liquid slug length gets shorter. On the other hand the pressure difference between the upper and lower vapors also increases, so that it is a clear explanation for this sudden flow jump. The second vapor behavior more clearly demonstrates the interfacial behavior. When the gap size between two vapors reduces to be smaller than a specified length, two vapors are to coalesce and merge into one. Such coalescence has not happened during the present calculation.

5. Discussions

The steady state calculation looks to be reasonable. As power generation goes up, the slope of the coolant temperature along the flow direction also increases. It drops near the top of the fuel slug

because there is no power generation. Generally, the process for vapor formation and initial vapor growth shows the physical behavior qualitatively as assumed in the present model. The initial vapor growth is similar to the results shown in CABRI analysis using FRAX-5 and SAS4A,[9] where the sudden enlargement of the vapor region downward was predicted within a short time, ~ ms. However, the abnormal behavior after ~2.3 second is not clearly understood at this time. Another point is that some user specified parameters such as the conditions for vapor formation, liquid gap distance for the vapor coalescence, time-step reduction criteria, liquid film thickness, wall heat transfer coefficient between the vapor and wall, etc. are not physically justified at this time.

In general, most of physical phenomena seem to be reasonable qualitatively so far, because a basis for complete sodium boiling model was confirmed through the analysis of the active fuel slug region in the former study. [11] The vapor pressure is quite sensitive to its volume change, and the balance between the wall and interface heat transfers also come out to be important to the vapor volume change. The flow reversal was predicted in the previous study,[9] but it has not been found in the present study. For resolving all unexplainable problems at this time, continuous model qualification and more sophisticated verification for the model should be followed.

It is learned from this analysis that sodium voiding develops so rapidly that large reactivity can be introduced in the core within a short time, and thus it may threaten the fuel integrity during accidents under which sodium boiling is anticipated. Therefore, it is very important to predict the phenomena accurately in order to understand the detailed fuel behavior due to the reactivity feedback.

Acknowledgement

This work was performed under the Long-term Nuclear R & D Programs sponsored by the Korea Ministry of Science and Technology.

Nomenclatures

Δw = Changes of liquid slug flow rates over a time-step

P_b = pressure at the bottom of the slug

P_t = pressure at the top of the slug

$Z_i(2,t,K)$, $Z_i(1,t,K)$ = Height of upper/lower liquid-vapor interfaces, repectively

$q_e(z,t)$ = Cladding-to-vapor heat flux

G = liquid mass flow rate (kg/s-m^2)

ρ_l = liquid density

k_l = Liquid thermal conductivity near interface

c_l = liquid specific heat

$\varphi(z,t)$ = wall heat flow per unit coolant volume (w/m^3)

$Q_c(z,t)$ = volume source due to direct heating by neutrons and gamma rays (w/m^3)

$\alpha = k_l / \rho_l C_l$, the thermal diffusivity of liquid sodium

c_l = liquid heat capacity

ρ_l = liquid density

Q = heat input per unit volume in the liquid

References

[1] Dohee, Hahn, et al., "KALIMER Preliminary Conceptual Design Report", KAERI/TR-1636/2000

[2] G.A. Greene, T. Ginsberg, and M.S. Kazimi, "Assessment of the Thermal Hydraulic Technology of the Transition Phase of a Core-Disruptive Accident in a LMFBR", NUREG/CR-3014, Nov. 1982

[3] Alan E. Waltar and Albert B. Reynolds, Fast Breeder Reactors II', Pergamon Press, New York, Oxford, Toronto, Sydney, Paris, Frankfurt, 1980

[4] F.E. Dunn, et al., "The SAS2A LMFBR Accident-Analysis Computer Code," ANL-8183, Oct. 1974

[5] Y.M. Kwon, et al., "SSC-K Code User's Manual (Rev. 0)", KAERI/TR-1619/2000

[6] Y.S. Tang, et al., "Thermal Analysis of Liquid-Metal Fast Breeder Reactors", ANS, 1978

[7] M. Green, "FRAX, A Whole Core Accident Code for Fast Reactors", AEA Presentations to KAERI, March 1998

[8] D.J. Brear, J.A. Moran, T. Rudge, "Fuel Pin loading and pin failure criteria in the UK code FRAX-5 under WCA condition", Fast Reactor Core and Fuel Structure Behavior, BNES, London, 1990

[9] T. Rudge, "Homsep-2 : A One-dimensional Sodium Boiling Model for the Fast Reactor", Nucl. Energy, 1989, 28, N0. 3, June, 171-181

[10] W.P. Chang, et al., "Development of Two-phase Flow, 'SOBOIL', for Sodium", . KAERI/TR-1636/2000

[11] W.P. Chang, et al., "Sodium Voiding Analysis in KALIMER", ICONE-9, Nice, France, April, 2001

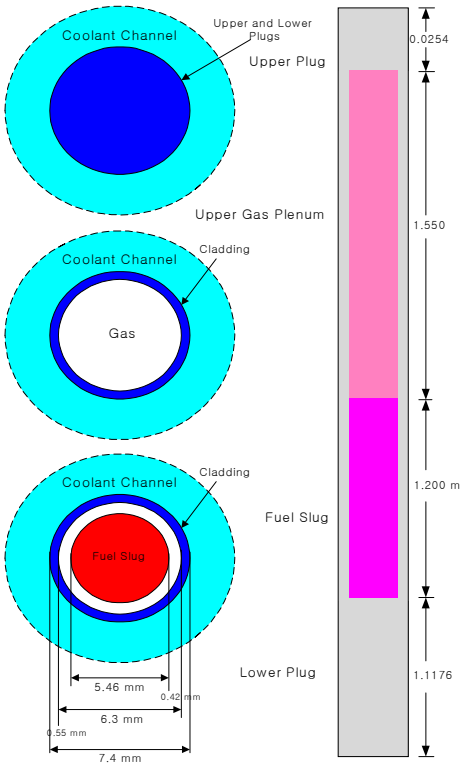

Fig. 5 Representation of the KALIMER Fuel Pin

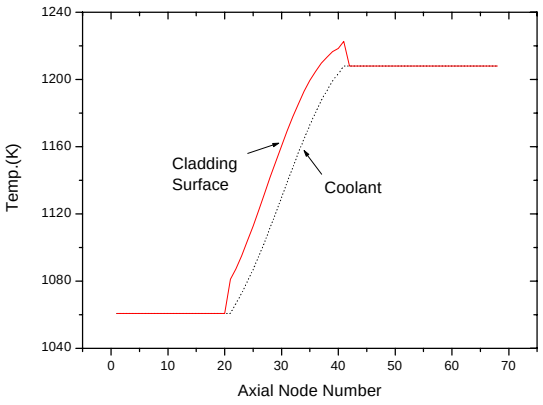

Fig. 6 Steady State Temperature Profiles

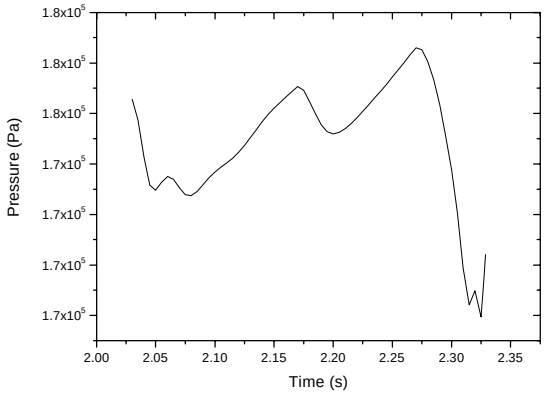

Fig. 7 Pressure Change for the First Vapor

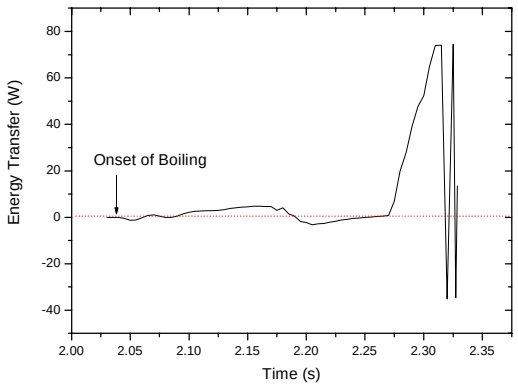

Fig. 8 Wall Heat Transfer (Vapor to Cladding)

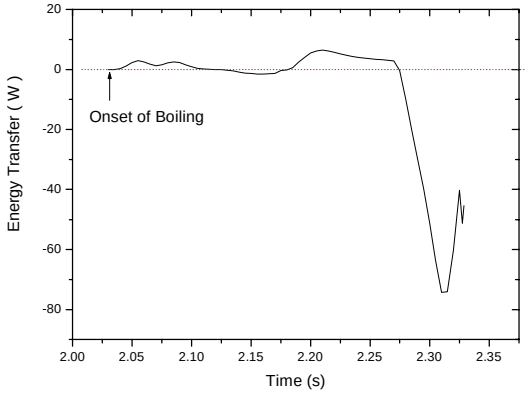

Fig. 9 Interface Heat Transfer (Vapor to Liquid)

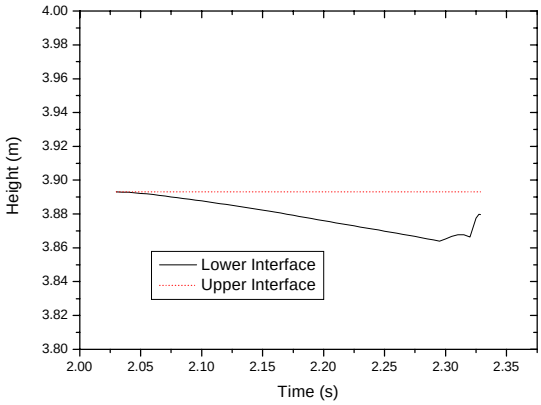

Fig. 10 Interface Behavior for the First Vapor

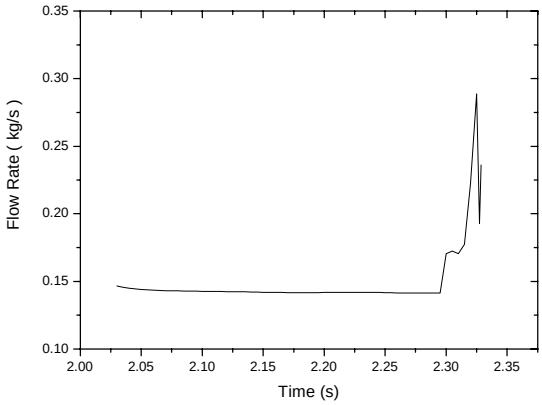

Fig. 11 Liquid Slug Flow Change (between First and Second Vapors)

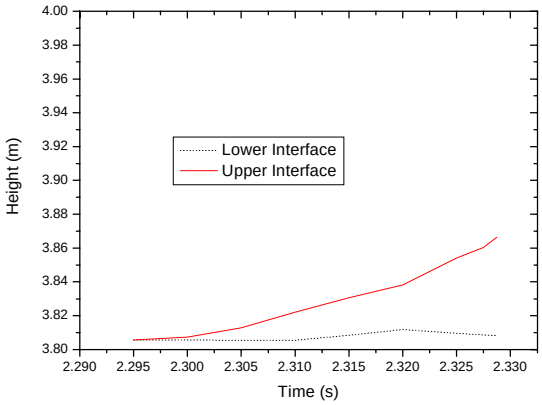

Fig. 12 Interface Behavior for the Second Vapor

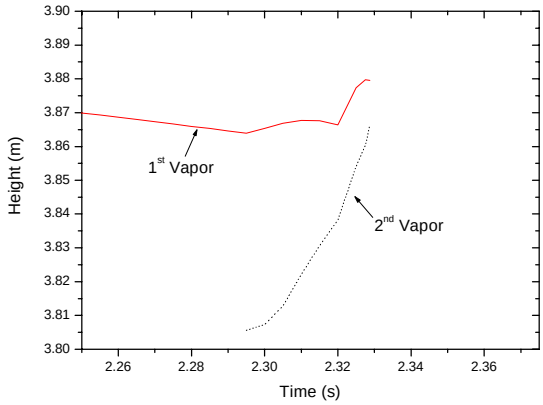

Fig. 13 Liquid Slug Gap Distance between Two Vapors

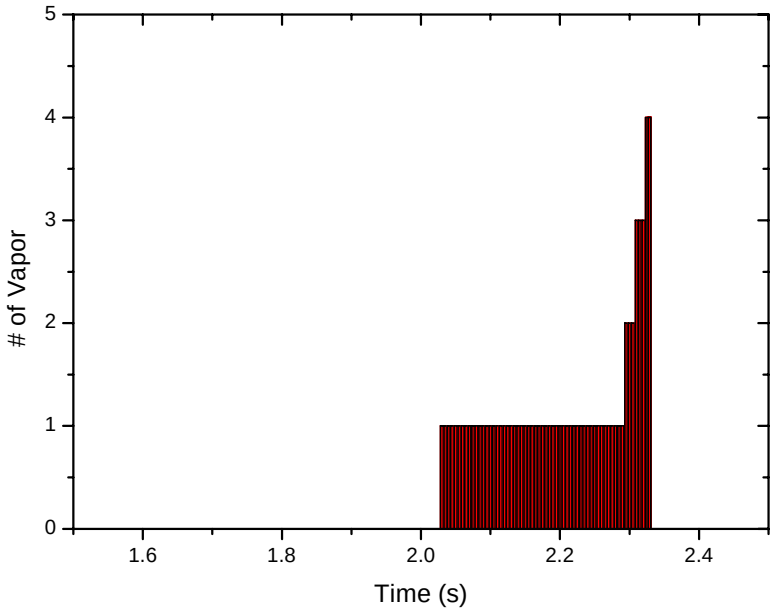

Fig. 14 Vapor Number Change with Time